Available online at www.sciencedirect.com
SCIENCE DIRECT®

Journal of the European Ceramic Society 24 (2004) 2055–2059

www.elsevier.com/locate/jeurceramsoc

Reinforcement by crack-tip blunting in porous ceramics

Zhen-Yan Deng[a,*], Jihong She[b], Yoshiaki Inagaki[a], Jian-Feng Yang[b], Tatsuki Ohji[b], Yoshihisa Tanaka[c]

[a]*Synergy Ceramics Laboratory, Fine Ceramics Research Association, Nagoya 463-8687, Japan*
[b]*Synergy Materials Research Center, National Institute of Advanced Industrial Science and Technology, Nagoya 463-8687, Japan*
[c]*Metal Matrix Composite Research Group, National Institute for Materials Science, 1-2-1 Sengen, Tsukuba, Ibaraki 305-0047, Japan*

Received 30 January 2003; accepted 17 May 2003

Abstract

A crack-tip blunting mechanism in porous ceramics was identified in this study. The reinforcement by crack tip blunting in porous ceramics was analyzed quantitatively, based on a grain fracture model. The investigation revealed that the crack tip blunting increases the fracture toughness of porous ceramics, depending on pore morphology and grain arrangement. The theoretical predictions were in good agreement with the experimental results.

Keywords: Modeling; Porous ceramics; Toughness and toughening; Crack blunting

1. Introduction

Porous ceramic materials have received considerable attention in the recent years, due to their wide applications in filters, sensors and catalyst supports[1,2] as well as lightweight structural components.[3–6] Usually, the mechanical properties of porous materials are not as good as the corresponding dense materials. To improve the mechanical properties of porous ceramics, it is important to understand the possible reinforcing mechanisms in these materials.

When a crack meets a pore in a porous ceramic material, as shown in Fig. 1, the crack tip becomes blunt. This decreases the stress-concentration at the crack tip and increases the external load to propagate the crack such that the fracture toughness increases. This is true especially for porous ceramics with open pores. In this study, a crack-tip blunting mechanism in porous ceramics is proposed. The main goal is to establish the relationship between the fracture toughness and pore morphology in porous ceramics.

* Corresponding author. Metal Matrix Composite Research Group, National Institute for Materials Science, 1-2-1 Sengen, Tsukuba, Ibaraki 305-0047, Japan. Tel.: +81-298-59-2238; fax: +81-298-59-2201.
E-mail address: deng.zhenyan@nims.go.jp (Z.-Y. Deng).

0955-2219/03/$ - see front matter © 2003 Elsevier Ltd. All rights reserved.
doi:10.1016/S0955-2219(03)00365-0

2. Model

Although the target of the present work is to get the dependence of fracture toughness on pore size and morphology, the model selects an ideal porous and dense ceramic for comparison, because in this case the model can more clearly show the pore blunting effect in porous ceramics. In the present model analysis, transgranular fracture is assumed to be predominant in porous and dense ceramics. A schematic representation of a sharp crack in dense material and a blunt crack in porous material is shown in Fig. 2(a) and (b). Macroscopically, the ceramic body is viewed as a uniform elastic medium, which obeys the elastic stress-field equations. The solution of the stress, σ_y, on the r-axis around a crack tip under a uniform tensile stress can be written as[7–10]

$$\sigma_y = \frac{K_I}{\sqrt{2\pi r}} \tag{1}$$

for a sharp crack and

$$\sigma_{y,blunt} = \frac{K_{I,blunt}}{\sqrt{2\pi r}} \frac{1+\rho_0/r}{(1+\rho_0/2r)^{3/2}} \tag{2}$$

for a blunt crack
where ρ_0 is the root radius of the blunt crack, which is half of the pore width at the crack tip, and $K_{I,blunt}$ is the

stress intensity factor at the blunt crack tip. The following analyses are based on the fact that the grain is an intact unit at the crack tip and it would fracture as an individual body. In fact, this concept has been used to simulate the crack propagation in dense ceramics.[11]

From Eqs. (1) and (2), it can be seen that the stress decreases with the distance away from the crack tip. This implies that the stress applied on a grain at the crack tip is not a constant, as shown in Fig. 2(c). However, the grain does not fracture immediately, even the stress at some positions exceeds its fracture strength, due to the stress dispersion and transfer.[12–14] As an approximation, the average stress on the grain is viewed as the fracture stress. In the practical three-dimensional situation, there is a distribution of the grain positions at the crack front. Therefore, a characteristic zone, $r_0 = d \sim 2d$, at the crack tip should be considered to calculate the average stress,[8] where d is an effective grain width at the crack tip. The size, $r_0 = 2d$, of the characteristic zone corresponds to a maximum deviated grain arrangement at the crack front (see the insets of Fig. 3).

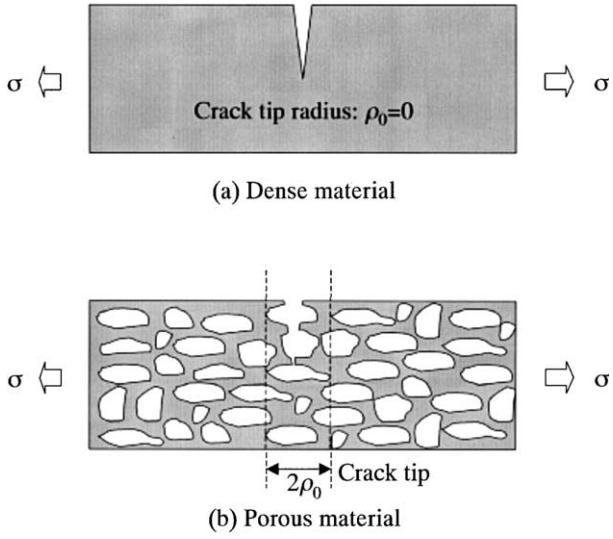

Fig. 1. Schematic representation of a crack propagated in (a) a dense ceramic material and (b) a porous ceramic material, showing a sharp crack-tip in the dense material and a blunt crack-tip in the porous material.

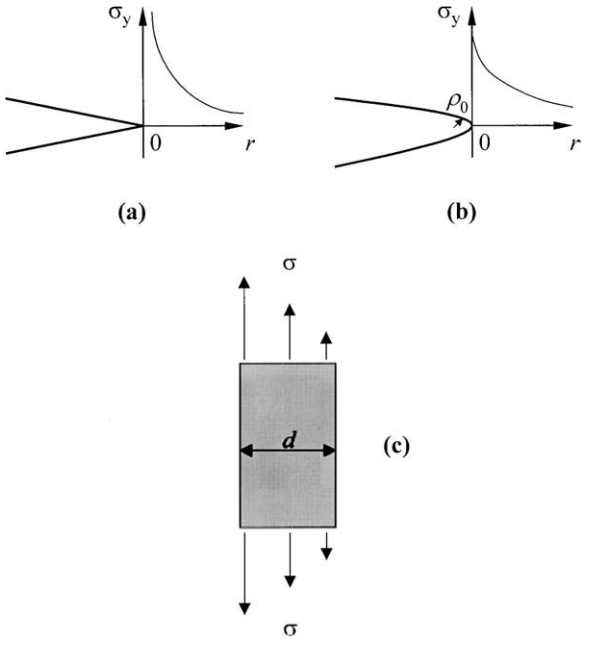

Fig. 2. Schematic representation of (a) a sharp crack, (b) a blunt crack with a root radius of ρ_0 and (c) a grain suffering a nonuniform tensile stress.

$$\bar{\sigma}_y = \left(\frac{1}{r_0}\right)\int_0^{r_0} \frac{K_I}{\sqrt{2\pi r}}\,dr = \frac{2K_I}{\sqrt{2\pi r_0}} \tag{3}$$

for a sharp crack and

$$\bar{\sigma}_{y,blunt} = \left(\frac{1}{r_0}\right)\int_0^{r_0} \frac{K_{I,blunt}}{\sqrt{2\pi r}} \frac{1+\rho_0/r}{(1+\rho_0/2r)^{3/2}}\,dr = \frac{2K_{I,blunt}}{\sqrt{2\pi(r_0+\rho_0/2)}} \tag{4}$$

for a blunt crack.

When the average stress on the grain exceeds a critical stress, σ_0, the fracture occurs and at the same time the crack starts to propagate. In fact, the critical stress is proportional to the fracture strength, σ_f, of the bulk specimen, that is

$$\sigma_0 = \alpha\sigma_f \tag{5}$$

where α is a constant related to the surface defect characteristics of the bulk ceramic specimen.

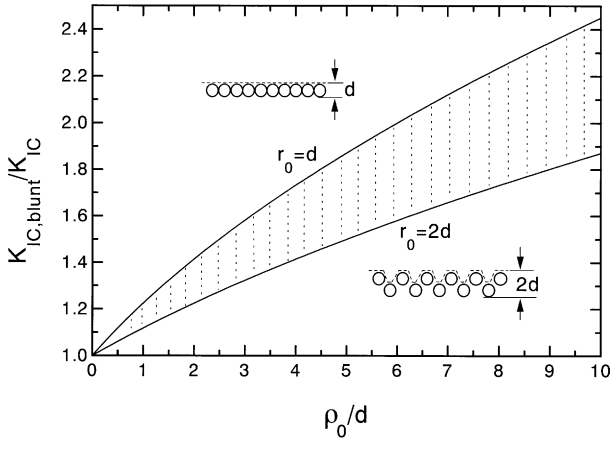

Fig. 3. Relationship between the toughness ratio of a blunt crack to a sharp crack and the ratio of the blunt crack-tip radius to the effective grain width, where the hatched region represents the results for different characteristic zone size. The dashed lines in the insets are the crack front of different grain arrangement.

If the resistance curve is not considered, the fracture toughness in dense and porous ceramics can be calculated by Eqs. (3)–(5). When the characteristic constant α and average grain width of dense and porous ceramics are approximately equal, the following relationship can be obtained

$$\frac{K_{IC,blunt}/K_{IC}}{\sigma_{f,blunt}/\sigma_f} = \left(1+\frac{\rho_0}{2r_0}\right)^{1/2}. \quad (6)$$

This indicates that the fracture toughness is not degraded as much as the fracture strength when the porosity is introduced into the ceramics. If the fracture strength of dense and porous ceramics is the same, then

$$\frac{K_{IC,blunt}}{K_{IC}} = \left(1+\frac{\rho_0}{2r_0}\right)^{1/2}. \quad (7)$$

The relationship in Eq. (7) is shown in Fig. 3, indicating that the crack-tip blunting obviously increases the fracture toughness of porous ceramics and that the larger the pore size at the crack front, the higher the fracture toughness of porous ceramics.

In order to compare the theoretical model with the experiment results quantitatively, two types of porous SiC with different pore morphologies were selected as follows, due to a negligible *R*-curve behavior for SiC ceramics with equiaxed grains.

3. Experimental

Two types of SiC powders were used in the experiments: one is a fine SiC powder (0.29 μm, Ibiden Co., Japan) and the other is a coarse SiC powder (2.3 μm, Showa Denko Co., Japan), referred to as FSC and CSC, respectively. The fine SiC powder was used to form the green body directly. The coarse SiC powder (56.25 vol.%) was mixed with a fine Al_2O_3 powder (18.75 vol.%; TM-DAR, 0.21 μm, Tamei Chemical Co., Japan) and some plate-like C particles (25 vol.%; 5.0 μm, Kojundo Chemical Lab. Co., Japan) in a highly pure ethanol solution and ball-milled for 24 h, using nylon balls, then dried and sieved using a 100-mesh nylon sieve. Green-body billets measuring 12 mm×55 mm×5.5 mm were prepared by single-ended pressing, under a pressure of ~50 MPa, in a stainless-steel die. The green-body billets were then sintered for 1 h in a furnace, in an air atmosphere, at a heating and cooling rate of 5 °C/min. The sintering temperatures for FSC and CSC billets were 1500 and 1450 °C, respectively.

The sintered specimens were cut into pieces measuring 3 mm×4 mm×40 mm and then ground and beveled before strength and toughness measurements. Strength was determined by three-point bend tests, with a span of 30 mm and a crosshead speed of 0.5 mm/min. Fracture toughness was measured by a chevron-notched-beam (CNB) technique.[15,16] Details of the CNB specimen geometry and testing procedures have been described elsewhere.[16] The shape of the ligament was a regular triangle with an edge length of 3 mm, and the initial crack length (a_0) was 1.4 mm. The width of the chevron notch was 0.1 mm, and the fracture testing was conducted by a three-point bending loading with a span of 16 mm and a crosshead speed of 0.05 mm/min. The fracture toughness was calculated by an equation developed by Sakaguchi et al.,[17] using the peak load of the load–displacement curve. At least five samples were used for each strength and toughness point.

The density of the sintered specimens was measured by the Archimedes method. The morphology and pore structure of the porous SiC were observed, using the fresh-fractured surface of the sample, by scanning electron microscopy (SEM). The pore size and effective grain width at the crack tip were measured by a line-intercept method.[18] At least 200 pores and grains on SEM micrographs were used to calculate the average pore size and grain width.

4. Results and discussion

As the crack produced by the CNB technique is the natural crack,[9] the crack tip width reflects the average pore size at the crack front and the measured fracture toughness is suitable for comparison with the present model. The grain and pore morphologies of the two types of porous SiC ceramics are shown in Fig. 4. It can be seen that the FSC specimen has fine pore structures, and the pores in the CSC specimen are large and have definite alignment. The aligned pores in the CSC specimen were produced by burning out the plate-like C particles, because the unidirectional pressing made the C particles align in the plane normal to the pressing direction in the green billets.

As we know, SiC particles do not grow at the present sintering temperatures of 1450 and 1500 °C.[19] Therefore, the bonding between the SiC particles was produced by oxidation-resultant other phases,[20–22] due to the sintering in an air atmosphere. In fact, our X-ray diffraction analyses showed that there were a strong crystallized SiO_2 phase in the FSC specimen and mullite, Al_2O_3 and crystallized SiO_2 phases in the CSC specimen. Although the compositions in the present porous SiC ceramics are complicated, both of the FSC and CSC specimens exhibited a transgranular fracture (Fig. 4); this is consistent with the assumption of the present model. In the practical calculation, the width of the bonding between the SiC particles also is viewed as the effective grain width at the crack tip.

Moreover, the effect of surface defects on the fracture strength of porous ceramics is different from that of

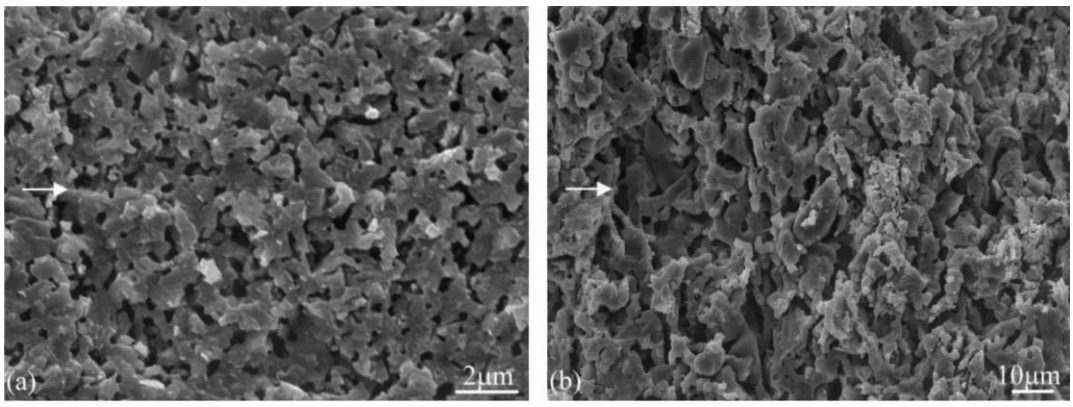

Fig. 4. SEM micrographs of grain and pore morphology in (a) FSC porous specimen and (b) CSC porous specimen, where the arrows represent crack propagation direction during strength and toughness tests.

dense ceramic materials. Recently, Flinn et al.[23] found that the size of surface defects has only a negligible influence on the strength of porous ceramics, especially for the specimens with high porosity. This is because there are more surface defects on porous ceramic specimens than on dense ceramic specimens.[24] The existence of pores and more surface defects greatly reduces the stress concentration at the surface cracks of porous ceramics (see Fig. 5 of Ref. 25).

Therefore, the surface defect related constant, α, can be viewed as the same for the present FSC and CSC specimens. Here, it can be seen that the comparison between the experiment and model by using different porous ceramics is better than that by using the dense and porous ceramics, because in dense ceramics the fracture strength greatly depends on the surface defect characteristics. From Eqs. (4) and (5), the following relationship between the fracture toughness and strength for the two types of SiC ceramics with different pore morphologies can be obtained

$$\frac{K_{IC}^{CSC}/\sigma_f^{CSC}}{K_{IC}^{FSC}/\sigma_f^{FSC}} = \left(\frac{r_0^{CSC}+\rho_0^{CSC}/2}{r_0^{FSC}+\rho_0^{FSC}/2}\right)^{1/2}. \quad (8)$$

Table 1
The parameters and mechanical properties of porous FSC and CSC ceramics

	FSC	CSC
Relative density	64.6%	63.6%
Effective grain width, d (μm)	0.47	2.50
Fracture strength, σ_f (MPa)	152.2±16.6	39.6±1.9
Fracture toughness, K_{IC} (MPa·m$^{1/2}$)	1.42±0.12	0.90±0.08
Pore width at crack tip, $2\rho_0$ (μm)	0.49	8.16
$\frac{K_{IC}^{CSC}/\sigma_f^{CSC}}{K_{IC}^{FSC}/\sigma_f^{FSC}}$ experimental	2.44	
$\frac{K_{IC}^{CSC}/\sigma_f^{CSC}}{K_{IC}^{FSC}/\sigma_f^{FSC}}$ theoretical	2.57 ($r_0=2d$)~2.77 ($r_0=d$)	

The relative density, fracture strength and toughness, effective grain width and average pore size of the two types of porous SiC ceramics are listed in Table 1. By using the parameters in Table 1, the experimental and theoretical values of the K_{IC}/σ_f ratio of the porous CSC and FCS ceramics were calculated and given in Table 1. The theoretical prediction is in good agreement with the experimental result. The higher K_{IC}/σ_f value in the porous CSC ceramic reflects the crack-tip blunting, due to the large-sized pores at the crack front. At the same time, the above results also indicate that the average stress on the grains at the crack front as the fracture stress is a good approximation, because part of the difference in the K_{IC}/σ_f value between the two different porous SiC ceramics comes from their different effective grain width. Moreover, the theoretical prediction by using the characteristic zone size, $r_0=2d$, is closer to experimental results, implying that the model that considers the grain position distribution at the crack front is more reasonable.

5. Conclusions

The crack-tip blunting reinforcement in porous ceramics was investigated, based on a grain fracture model. The investigation revealed that crack tip blunting increased the fracture toughness of the porous ceramics, to an extent depending on the pore morphology. The larger the pore size at the crack front, the higher the fracture toughness of the porous ceramic relative to its fracture strength. The theoretical predictions were in agreement with the experimental results.

Acknowledgements

This work was supported by NEDO, as part of the Synergy Ceramics Project promoted by the Agency of Industrial Science and Technology (AIST), Ministry of

International Trade and Industry (MITI), Japan. The authors are members of the Joint Research Consortium of Synergy Ceramics.

References

1. Deng, Z. Y., Fukasawa, T., Ando, M., Zhang, G. J. and Ohji, T., High-surface-area alumina ceramics fabricated by the decomposition of $Al(OH)_3$. *J. Am. Ceram. Soc.*, 2001, **84**, 485–491.
2. Deng, Z. Y., Fukasawa, T., Ando, M., Zhang, G. J. and Ohji, T., Bulk alumina support with high tolerant strain and its reinforcing mechanisms. *Acta Mater.*, 2001, **49**, 1939–1946.
3. Hardy, D. and Green, D. J., Mechanical properties of a partially sintered alumina. *J. Eur. Ceram. Soc.*, 1995, **15**, 769–775.
4. Deng, Z. Y., Fukasawa, T., Ando, M., Zhang, G. J. and Ohji, T., Microstructure and mechanical properties of porous alumina ceramics fabricated by the decomposition of aluminum hydroxide. *J. Am. Ceram. Soc.*, 2001, **84**, 2638–2644.
5. Deng, Z. Y., Yang, J. F., Beppu, Y., Ando, M. and Ohji, T., Effect of agglomeration on mechanical properties of porous zirconia fabricated by partial sintering. *J. Am. Ceram. Soc.*, 2002, **85**, 1961–1965.
6. Corbin, S. F. and Apte, P. S., Engineered porosity via tape casting, lamination and the percolation of pyrolyzable particulates. *J. Am. Ceram. Soc.*, 1999, **82**, 1693–1701.
7. Okamura, H., *Introduction to Linear Fracture Mechanics*. Baifukan, Tokyo, 1976.
8. Usami, S., Kimoto, H., Takahashi, I. and Shida, S., Strength of ceramic materials containing small flaws. *Eng. Fract. Mech.*, 1986, **23**, 745–761.
9. Awaji, H. and Sakaida, Y., V-notch technique for single-edge notched beam and chevron notch methods. *J. Am. Ceram. Soc.*, 1990, **73**, 3522–3523.
10. Awaji, H., Choi, S. M. and Jayaseelan, D. D., Indirect estimation of critical frontal process-zone size using a single-edge V-notched-beam technique. *J. Ceram. Soc. Japan*, 2001, **109**, 591–595.
11. Cao, J. W. and Sakaida, Y., Microscopic simulation of microcrack propagation in Al_2O_3 ceramic composites. *Ceram. Eng. Sci. Proc.*, 2001, **22**, 299–306.
12. Timoshenko, S. P. and Goodier, J. N., *Theory of Elasticity*. McGraw-Hill, New York, 1985.
13. Bai, T., Pollard, D. D. and Gao, H., Explanation for fracture spacing in layered materials. *Nature*, 2000, **403**, 753–756.
14. Deng, Z. Y., Zhang, G. J., Ando, M. and Ohji, T., Model analysis of multicrack mechanisms in ceramic/superplastic laminates. *J. Am. Ceram. Soc.*, 2002, **85**, 1793–1803.
15. Ohji, T., Shigegaki, Y., Miyajima, T. and Kanzaki, S., Fracture resistance behavior of multilayered silicon nitride. *J. Am. Ceram. Soc.*, 1997, **80**, 991–994.
16. Ohji, T., Hirao, K. and Kanzaki, S., Fracture resistance behavior of highly anisotropic silicon nitride. *J. Am. Ceram. Soc.*, 1995, **78**, 3125–3128.
17. Sakaguchi, S., Murayama, N., Kodama, Y. and Wakai, F., Equation for the evaluation of fracture toughness by chevron notched beam with using JIS type bending bar specimen. *J. Ceram. Soc. Japan*, 1991, **99**, 47–51.
18. Deng, Z. Y., Shi, J. L., Zhang, Y. F., Lai, T. R. and Guo, J. K., Creep and creep-recovery behavior in silicon-carbide-particle-reinforced alumina. *J. Am. Ceram. Soc.*, 1999, **82**, 944–952.
19. Zhou, Y., Hirao, K., Toriyama, M., Yamauchi, Y. and Kanzaki, S., Effects of intergranular phase chemistry on the microstructure and mechanical properties of silicon carbide ceramics densified with rare-earth oxide and alumina additions. *J. Am. Ceram. Soc.*, 2001, **84**, 1642–1644.
20. She, J. H., Ohji, T. and Deng, Z. Y., Thermal shock behavior of porous silicon carbide ceramics. *J. Am. Ceram. Soc.*, 2002, **85**, 2125–2127.
21. She, J. H., Deng, Z. Y., Jayaseelan, D. D. and Ohji, T., Oxidation bonding of porous silicon carbide ceramics. *J. Mater. Sci.*, 2002, **37**, 3615–3622.
22. She, J. H., Yang, J. F., Kondo, N., Ohji, T., Kanzaki, S. and Deng, Z. Y., High-strength porous silicon carbide ceramics by an oxidation-bonding technique. *J. Am. Ceram. Soc.*, 2002, **85**, 2852–2854.
23. Flinn, B. D., Bordia, R. K., Zimmermann, A. and Rodel, J., Evolution of defect size and strength of porous alumina during sintering. *J. Eur. Ceram. Soc.*, 2000, **20**, 2561–2568.
24. Deng, Z. Y., Zhou, Y., Inagaki, Y., Ando, M. and Ohji, T., Role of $Zr(OH)_4$ hard agglomerates in fabricating porous ZrO_2 ceramics and the reinforcing mechanisms. *Acta Mater.*, 2003, **51**, 731–739.
25. Rice, R. W., Limitations of pore-stress concentrations on the mechanical properties of porous materials. *J. Mater. Sci.*, 1997, **32**, 4731–4736.